outer potential flow and the boundary-layer modifies the pressure distribution and the boundary-layer thickness, to finally impart such a shape to the equivalent contour as to render the streamline curvature at the trailing edge finite: i.e., the singular α^* of the resulting contour always coincides with the actual angle of attack.

Analogy with the Jet-Flap

If a streamline is curved, a normal pressure gradient develops; but, to avoid possible confusion, it must be stressed that such a gradient is present everywhere within the flowfield, even in potential flow, and there is nothing to worry about. No supplementary terms have to be introduced in order to account for the effects of streamline curvature. However, within the boundary layer and the wake, the situation changes, as the Bernoulli constant is not the same throughout the flowfield. One way to understand the phenomena involved is to introduce an analogy with a jet-flap: i.e., the wake emerging from the trailing edge may be imagined to act as a jet having a negative momentum, equal precisely to the airfoil drag, $J = -\rho/2U_\infty^2 C_D$. We note that this analogy has been first put to light as early as 1957.[5]

Then, any theory of jet-flapped airfoils may be used to assess the effect upon the lift of the wake curvature: since the equivalent jet intensity is weak, a simplified method would do the job. Such a theory was developed in Ref. 6; there, the jet was replaced by a vortex sheet, along which a circulation distribution is placed, related to the pressure differential Δp across the jet. This normal force is supported by the jet through the deflection of its momentum vector $\boldsymbol{J}$, and here the local streamline (or wake) curvature enters into play:

$$\Delta p = J/\bar{r}_s \tag{2}$$

As, in our case, the equivalent jet coefficient is negative ($-C_D$), the vortices distributed along the wake have negative intensities; finally, one finds for the lift slope:

$$C_{L\alpha} \cong 2\pi\alpha(1 - C_D/4) \tag{3}$$

In the absence of massive separation, for typical airfoils, C_D is of the order of 0.01, therefore, the above negative correction (due only to the wake curvature) is quite small. We remark that, from the data of Ref. 1 it would appear that taking the wake curvature into account would produce an increase in lift, a result which is difficult to understand.

Discussion

Obviously, the effect upon the lift of the vorticity distribution along the wake, due to its curvature as predicted by the jet-flap analogy, is small and can be neglected, for all intents and purposes. Then, two questions arise:

The first question is what is the reason for this loss of lift? In fact, almost all procedures embodying viscous-inviscid coupling provide fair estimates of the lift slope,[3] even without taking the wake-curvature effects explicitly into account. A physical image of the phenomena involved may be envisaged as follows: due to the pressure distribution, the boundary-layer development is such that, usually, at the trailing edge (where local separation is often present), its upper surface thickness is much larger than on the lower surface (Fig. 1) and, in addition, this dissymmetry increases with α. Considering now the skeleton of the equivalent (blunt) airfoil, one may see that it has a lower incidence and less camber than the original contour, thus producing less lift. The requirement for removal of wake-curvature singularity (see above) results in the equivalent contour having, in addition, less aft-loading[4] and a negative effective camber towards the trailing edge,[2] which also contribute to the lift loss. We conclude, therefore, that the reduction in lift slope can be accounted for by the effect of the boundary-layer thickness alone, without invoking the curvature of the wake.

The second question to be addressed is what is then, albeit small, the main effect of the wake curvature to be embodied in a consistent theory? The answer lies in the way in which the Kutta condition is to be imposed. At the physical trailing edge (point A in Fig. 1), the pressure must be single-valued, p_A; then, one of the basic assumptions of boundary-layer theory (constant pressure across the thickness), would require that the same pressure should prevail also at points B and C, the upper- and lower-surface edges of the equivalent blunt contour. It is here that the wake curvature enters into play, for a correct formulation of the Kutta condition: namely, between the edges of the wake, a pressure differential, $p_B - p_C$, has to be imposed:

$$p_B - p_C = \rho U_\infty^2 C_D/(2\bar{r}_s) \tag{4}$$

This implies, of course, departing from the first-order boundary-layer theory which, at the trailing edge, becomes questionable anyway. How to implement the ideas put forward here is, however, another story.

References

[1]Coiro, D. P., de Matteis, P., and Amato, M., "Wake Effects on the Prediction of Transonic Viscous Flow Around Airfoils," *Journal of Aircraft*, Vol. 29, No. 3, 1992, pp. 437–443.

[2]Dumitrescu, L. Z., "Flow Near the Trailing Edge of an Airfoil," *AIAA Journal*, Vol. 30, No. 4, 1992, pp. 865–870.

[3]Cebeci, T., "Essential Ingredients of a Method for Low Reynolds-Number Airfoils," *AIAA Journal*, Vol. 27, No. 12, 1989, pp. 1680–1688.

[4]Ormsbee, A. I., and Maughmer, M. D., "A Class of Airfoils Having Finite Trailing-Edge Pressure Gradients," *Journal of Aircraft*, Vol. 23, No. 2, 1986, pp. 97–103.

[5]Patraulea, N. N., Dumitrescu, L. Z., Popescu, C., Caprita, D., and Gab, H., "Recherches Experimentales sur les Profils d'Ailes Soufflés," *Revue de Mécanique Appliquée* (a publication of the Romanian Academy of Sciences), Bucharest, Romania, Vol. 2, No. 2, 1957, pp. 21–42 (in French).

[6]Patraulea, N. N., Dumitrescu, L. Z., and Caprita, D., "Caractéristiques Aérodynamiques des Profils à Volet Fluide," *Revue de Mécanique Appliquée*, Bucarest, Vol. 3, No. 3, 1958, pp. 215–231 (in French).

Tail Load Calculations for Light Airplanes

E. V. Laitone*
University of California, Berkeley, California 94720

Introduction

MOST airplanes have a download on their rear tail in order to balance the nose-down pitching moment produced by their cambered wing. This is the usual case, because the wing profile curvature required for good wing stall unfortunately produces a nose-down pitching moment. The negative pitching moment coefficient ($C_M < 0$) is a pure couple that is independent of the unstalled lift coefficient ($C_L < C_{L,\max}$), and remains constant for any center of gravity (c.g.) location. As shown in Fig. 1, this nose-down couple must be

Received Sept. 25, 1992; revision received Jan. 21, 1993; accepted for publication March 10, 1993.

*Professor Emeritus, Department of Mechanical Engineering. Fellow AIAA.

balanced by a tail download; Naylor[1] and Laitone[2] show how severely this increases the induced drag of the airplane. Durand[3] states that the optimum design goal is to reduce the required tail download to nearly zero. Figure 1 indicates how the tail download could be decreased by moving the c.g. aft so that the wing lift will produce a nose-up moment when the c.g. is behind the wing's aerodynamic center (ac $\approx \frac{1}{4}$). However, this nose-up moment from the wing's lift is limited by the fact that the airplane's longitudinal oscillations become unstable if the c.g. is aft of the neutral point (np), which is well ahead of the wing's midchord for most airplanes. Because of this limitation on the aft c.g. location, the only method for further reducing the tail download is to alter the wing's camber line so as to have $C_{M,ac}$ less negative, but still have good stall characteristics. This was first attempted by Munk[4] when he developed the reflexed (*s*-shape) camber line for the NACA-M airfoil profiles. The effectiveness of the reflexed camber line is shown in Fig. 2 for the NACA-4412 airfoil. A large negative pitching moment coefficient ($C_{M,ac} = -0.09$), was reduced to zero by the moderate upward reflex given by the dotted line in Fig. 2.

Unfortunately, most of the recent airfoil profiles designed for light airplanes, such as the Wortman[5] or the NASA-General Aviation,[6] have an extremely large nose-down pitching moment ($C_{M,ac} \approx -0.18$). This is a direct consequence from the development of a camber line that would produce a smooth $C_{L,max} \approx 2$, and a large lift-drag ratio at the design lift coefficient (C_L) for the desired cruise speed. If these types of airfoils must be used, then it is recommended that if a zero tail load cannot be attained at cruise speed, then an inverted camber profile be used for the rear tail. The inverted camber tail would always provide the airplane with a nose-up pitching moment at any c.g. location. The inverted camber should be selected to have the design $C_{L,t}$ match that for the tail download occurring at the desired speed.

However, the optimum design procedure for a given airplane design would be to select the cambered wing so that the so-called "trim-drag" of the complete airplane was considered as important as the lift-drag ratio of the wing alone. This consideration is important because any tail download increases the induced drag of both the wing and the tail.

Fortunately, for the typical light airplane with its small rear tail, and a nearly rectangular wing planform with an aspect ratio A of at least five ($A \geq 5$), very simple relations can be developed to aid in either the design stage, or in the trim condition of a given light airplane to decrease the tail download, and increase the lift to drag ratio of some light airplanes by nearly 5%.

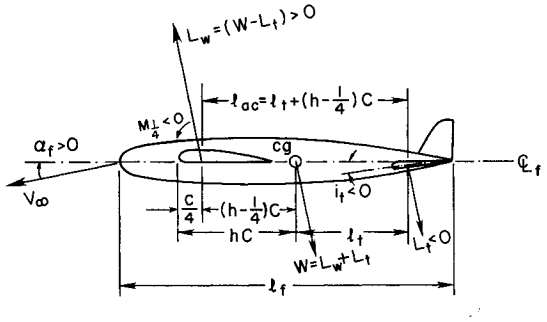

Fig. 1 Sign conventions for terms in Eqs. (1–3).

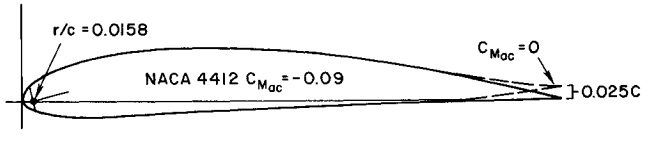

Fig. 2 Effect of *S*-camber line on the NACA-4412 airfoil.

Tail Load Calculation

The explicit relations that will now be derived are also applicable to all conventional sail planes, and they immediately show how much the tail download can be decreased by either moving the c.g. aft, or by decreasing the airplanes nose-down couple. As shown by Perkins and Hage,[7] the moments produced by the drag components of the wing and the tail can be neglected for $C_L < 1$. Consequently, for most light airplanes in steady flight, the moment balance about their c.g. (Fig. 1) is given by

$$M_{c.g.} \approx M_{1/4} + M_f + L_w(h - \tfrac{1}{4})c - l_t L_t \qquad (1)$$

The nondimensional $h = (X_{c.g.}/c)$, where $X_{c.g.}$ is the distance of the c.g. behind the leading edge of the wing's mean aerodynamic chord c, and $M_{1/4}$ represents the nose-down couple produced by the cambered wing. M_f is the unstable couple produced by the fuselage, which is usually neglected even though it can decrease longitudinal stability by as much as 10% in some airplanes. A conservative estimate for M_f is given by Perkins and Hage,[7] for the usual case where less than 40% of the fuselage is in front of the wings, as

$$M_f \approx l_f w_f^2 q \alpha_f = C_{M,f} q S \bar{c} \qquad (2)$$

where l_f = fuselage length, $w_f \approx$ fuselage width, $q = \frac{1}{2}\rho V^2$, S = wing planform area, and α_f is the fuselage angle of attack as shown in Fig. 1. Note that a nose-up fuselage angle of attack ($\alpha_f > 0$) produces a nose-up couple that helps decrease the tail download.

For static longitudinal stability we must have $dM_{c.g.}/d\alpha < 0$, and this will be used later to locate the np which limits the aft location of the c.g. However, the simplest relation for the tail load in steady flight can be obtained by taking the moments about the wing's aerodynamic center (ac $\approx \frac{1}{4}$, Fig. 1), to obtain

$$M(h = \tfrac{1}{4}) = 0 \approx M_{1/4} + M_f + W(h - \tfrac{1}{4})c - l_{ac} L_t \qquad (3)$$

This moment balance, which cannot be used to determine longitudinal stability, is better for tail load calculations since the varying wing lift ($L_w = W - L_t$), has been replaced by the constant aircraft weight (W, which is only affected by fuel consumption). Also the varying tail length l_t has been replaced by the constant distance (lac) between the aerodynamic centers of the wing and tail, since

$$\text{lac} = l_t + (h - \tfrac{1}{4})c = \text{const.} \qquad (4)$$

After introducing the standard aerodynamic coefficients

$$C_{L,c.g.} = W/qS$$
$$C_{M,1/4} = M_{1/4}/qSc \qquad (5)$$

into Eq. (3), the tail load L_t is given by

$$L_t/W = [(h - \tfrac{1}{4}) + (C_{M,wb}/C_{L,c.g.})](c/\text{lac}) \qquad (6)$$

where

$$C_{M,wb} = C_{M,1/4} + C_{M,f}$$

It is important to note that although $C_{M,1/4}$ is a constant, $C_{M,f}$ varies with α_f as given by Eq. (2), and can only be calculated from the wings lift coefficient, as given by

$$C_{L,w} = (L_w/qS) = a_w(\alpha_f + i_w - \alpha_0) \qquad (7)$$

where

$$a_w = a_\infty/(1 + 2/A_w); \qquad A_w = b^2/S$$

Table 1 Effect of $C_{m,1/4}$ on tail load

$C_{m,1/4}$	α_0, α_f, deg	Lt/W	$V\sqrt{\alpha}$ (kt)	$C_{b,c.g.}$	$C_{L,t}$	i_t, deg
−0.01	−1, 4.01	0.0147	97	0.418	0.0341	0.99
−0.045	−2, 3.01	−0.0332	99	0.399	−0.0736	−1.63
−0.09	−4, 1.01	−0.108	103	0.372	−0.223	−1.89
−0.18	−4, 1.01	−0.252	109	0.329	−0.461	−5.51

W = 2000 lb, S = 150 ft^2, c = 5 ft, A_w = 6, lac = 10.5 ft, S_t = 27 ft^2, A_t = 3, l_f = 20 ft, w_f = 3.5 ft, $h = \frac{1}{4}$, $C_{L,w}$ = 0.412, i_w = 0.

The lift-curve slope a_∞ is the two-dimensional value corresponding to infinite aspect ratio A_w. As shown by Laitone,[8] a_∞ should not be used in the denominator of a_w. $\alpha_0 < 0$ is the zero lift angle for the wing, e.g., $\alpha_0 = -4$ deg for the NACA 4412 airfoil in Fig. 2. i_w is the angle of incidence of the wings chord line with respect to the fuselage reference line for α_f. As shown in Fig. 1, $i_w \approx 0$ for most light airplanes so that at cruising speed $\alpha_f \approx 0 \approx i_w$, and we have

$$C_{L,w} \approx a_w(-\alpha_0)$$

$$C_{M,\text{wb}} \approx C_{M,1/4} < 0$$

Then for zero tail load ($L_t = 0$) the c.g. must be moved aft so that for $C_{M,1/4} < 0$, $(X_{\text{c.g.}}/c) = h \approx (\frac{1}{4}) - C_{M,1/4}/C_{L,\text{c.g.}}$, which is usually an unstable c.g. location unless $C_{M,1/4}$ is very small in magnitude. However, if α_f as calculated from Eq. (7) is not negligible, we must calculate M_f and $C_{M,f}$ from Eq. (2), and add this to $C_{M,\text{wb}}$ in Eq. (6) in order to calculate the new tail load (L_t). This requires a second calculation for α_f from Eq. (7) since the wing lift is changed by $L_w = W - L_t$. This leads to a convergent iteration solution even for large α_f. However, the usual α_f is sufficiently small so that not even a third calculation for α_f is necessary. Again, it should be noted that $\alpha_f > 0$ decreases the tail download.

The calculations for the tail load on a typical light airplane are given in Table 1 by starting with $C_{L,w}$ given, and α_f a constant given by Eq. (7), so that now no iteration is required. This procedure evolved from replacing $C_{L,\text{c.g.}}$ in Eq. (6) by $C_{L,w} = C_{L,\text{c.g.}}(1 - Lt/W)$ to obtain

$$\frac{Lt}{W} = \frac{h - \frac{1}{4} + (C_{M,\text{wb}}/C_{L,w})}{(\text{lac}/c) + (C_{M,\text{wb}}/C_{L,w})} \tag{8}$$

Now we can calculate the exact value of Lt/W from Eq. (8), and then find the corresponding steady-state velocity V from

$$\frac{1}{2}\rho V^2 = \frac{W}{C_{L,\text{c.g.}}S} = \frac{W}{C_{L,w}S}\left(1 - \frac{Lt}{W}\right) \tag{9}$$

Calculation of Neutral Point

As previously mentioned, one must return to Eq. (1) in order to determine the static longitudinal stability. Introducing the aerodynamic coefficients [Eq. (5)] into Eq. (1) and noting that $C_{M,1/4}$ is constant, while $C_{M,f}$ varies with α_f as given in Eq. (2), and $C_{L,t} = L_t/q_tS_t = a_t(\alpha_f + i_t - \varepsilon)$, one obtains

$$\frac{dC_{M,\text{c.g.}}}{d\alpha_f} = \frac{l_f w_f^2}{cS} + a_w\left(h - \frac{1}{4}\right) - a_t\left(1 - \frac{d\varepsilon}{d\alpha}\right)V_h \tag{10}$$

where

$$V_h = \frac{l_t}{c}\frac{S_t}{S}\frac{q_t}{q} \tag{11}$$

The term ε is the downwash angle produced by the wing's trailing vortex system acting on the tail. The approximation $\varepsilon \approx 2C_{L,w}/\pi A_w$ is sufficiently accurate for most light airplanes with a small tail as long as $l_{ac} \geq (b/2)$ = wing semispan. It is the theoretical downwash in the so-called Treftz-plane for any wing having the ideal elliptic spanwise lift distribution.

Equation (10) is simplified by introducing the lift-curve slope, and the following relations:

$$a = \frac{dC_L}{d\alpha} = \frac{a_\infty}{1 + 2/A}; \qquad \frac{a_t}{a_w} = \frac{1 + 2/A_w}{1 + 2/A_t}$$

$$\frac{d\varepsilon}{d\alpha} = \frac{2}{\pi A_w}a_w \leq \frac{4}{2 + A_w}; \qquad a_\infty \leq 2\pi \tag{12}$$

A conservative estimate of longitudinal stability is then given by

$$\frac{dC_{M,\text{c.g.}}}{dC_{L,w}} = \frac{dC_{M,\text{c.g.}}}{d\alpha_f}\Big/a_w = h - \frac{1}{4} - V_h\left(\frac{1 - 2/A_w}{1 + 2/A_t}\right) + \frac{l_f w_f^2}{cSa_w}$$

$$V_h = \frac{l_t}{c}\frac{S_t}{S}\frac{q_t}{q} = \left(\frac{\text{lac}}{c} + \frac{1}{4} - h\right)\frac{S_t}{S}\frac{q_t}{q} \tag{13}$$

Most aeronautical texts let V_h be the constant given by the above when $h = \frac{1}{4}$, however, this results in the np being farther aft than it should be if the decrease in l_t is considered. The np is given by Eq. (13) when $dC_M/dC_L = 0$, as

$$h_{\text{np}} = \frac{1}{4} + \left[K\left(\frac{\text{lac}}{c}\right) - \frac{l_f w_f^2}{cSa_w}\right]\Big/(1 + K) \tag{14}$$

where

$$K = \left(\frac{1 - 2/A_w}{1 + 2/A_t}\right)\frac{S_t}{S}\frac{q_t}{q}$$

Calculation of Tail Incidence Angle

The required tail angle of incidence i_t, as shown in Fig. 1, can be calculated from

$$i_t = (C_{L,t}/a_t) - \alpha_f + (2C_{L,w}/\pi A_w)$$

An explicit relation for i_t can also be obtained by introducing Eqs. (11) and (12) into the previous Eqs. (1–5) so that

$$V_h a_t i_t = C_{M,1/4} + \left(\frac{l_f w_f^2}{cS} - V_h a_t\right)\alpha_0 + C_{L,w} \times \left[h - \frac{1}{4} + \frac{l_f w_f^2}{cSa_w} - V_h\left(\frac{1 - 2/A_w}{1 + 2/A_t}\right)\right] \tag{15}$$

The calculated i_t would give the angle of incidence shown in Fig. 1 for an all-movable tail. If a fixed tail with a movable elevator with deflection δ was used, then

$$i_t = i_{t,0} - \delta\left(\frac{\partial i_t}{\partial \delta}\right)$$

where values of the elevator effectiveness, $\partial i_t/\partial\delta$, are given in Ref. 7.

Discussion

In Table 1 the row $C_{M,1/4} = -0.09$ corresponds to a light airplane with a NACA-4412 airfoil, while the bottom row $C_{M,1/4} = -0.18$, represents the same airplane with a typical Wortman airfoil. Similar calculations show that at the same airspeed the use of the Wortman airfoil would nearly double the tail download. Equation (8) predicts $L_t = 0$ for $h = 0.454$ with the NACA-4412 airfoil. However, Eqs. (13) and (14) show that this is unstable since $h_{np} = 0.3264$, for $q_t/q = 1$.

References

[1]Naylor, C. H., "Notes on the Induced Drag of Wing-Tail Combination," British R&M 2528, July 1946.

[2]Laitone, E. V., "Positive Tail Loads for Minimum Induced Drag of Subsonic Aircraft," *Journal of Aircraft*, Vol. 15, No. 12, 1978, pp. 837–842.

[3]Durand, W. F., *Aerodynamic Theory*, Vol. 4, Springer-Verlag, Berlin, 1934, pp. 85, 86.

[4]Munk, M. M., *Fundamentals of Fluid Dynamics for Aircraft Designers*, Ronald Press, New York, 1929, pp. 76–83.

[5]Liu, H.-T., "Unsteady Aerodynamics of a Wortman Wing at Low Reynolds Numbers," *Journal of Aircraft*, Vol. 29, No. 4, 1992, pp. 532–539.

[6]McGhee, R. V., and Beasley, W. D., "Low-Speed Aerodynamic Characteristics of a 17-Percent Thick Airfoil Section Designed for General Aviation Applications," NASA TN D-7428, Dec. 1973.

[7]Perkins, C. D., and Hage, R. E., *Airplane Performance Stability and Control*, Wiley, New York, 1949, pp. 218, 229, 250.

[8]Laitone, E. V., "Lift Curve Slope for Finite-Aspect-Ratio Wings," *Journal of Aircraft*, Vol. 26, No. 8, 1989, pp. 789, 790.

Pressure Measurements on a Forward-Swept Wing-Canard Configuration

Giovanni Lombardi*
University of Pisa, Pisa 56126, Italy
and
Mauro Morelli†
CSIR Laboratory, Pretoria 0001, South Africa

Nomenclature

b = wing span, m
C_L = lift coefficient of the wing
$C_{L\alpha}$ = slope of the wing lift coefficient at low incidence
$C_{L\max}$ = maximum lift coefficient of the wing
C_l = wing sectional lift coefficient
$C_{l\alpha}$ = slope of the wing sectional lift coefficient at low incidence
c = chord length, m
c_p = pressure coefficient
L = stagger, horizontal distance between the points at $x/c = 0.3$ of the chords of the wing and the canard, at the root section, m
M = Mach number
T = gap, vertical distance between the points at $x/c = 0.3$ of the chords of the wing and the canard, at the root section, m
x = distance measured from wing section leading edge, m
y = distance along the span measured from wing root, m
α = angle of attack
α_{st} = angle of attack of maximum lift
γ = decalage, angle defined by the directions of the wing and canard chords, Fig. 1
Δc_p = pressure coefficient jump across the shock wave
η = $y/(b/2)$
Λ = angle of sweep at $\frac{1}{4}$ of the chord

Received Dec. 14, 1992; revision received March 25, 1993; accepted for publication March 25, 1993.

*Assistant Professor, Department of Aerospace Engineering, Diotisalvi, 2.

†Research Engineer, Medium Speed Wind Tunnel, P.O. Box 395.

Introduction

IN Ref. 1, the effects of a fore sweep, in the subsonic and transonic regimes, are studied; one of the main features arising from that analysis is that, as could be expected, the flow on a forward-swept wing separates first in the root region. This suggests the inclusion of some aerodynamic devices producing a favorable interference effect in that region (e.g., a lifting canard or a strake), in order to obtain a more uniform stall condition along the span. This could give a further advantage in the use of a forward-swept wing, which provides, in any case, the potential for increasing aerodynamic efficiency.[2]

For low angles of attack and low subsonic flows, the study of the canard-wing configurations, with fairly accurate results, can be performed by means of nonlinear potential numerical methods,[3–6] but, for high Mach numbers or high angles of attack, experiments are necessary, at least at the present state of the computational capabilities.

Experimental Setup

Pressure measurements on 320 points of the wing surface, as detailed described in Refs. 1 and 7, were carried out in the Medium Speed Wind Tunnel of the CSIR Laboratories, in South Africa. This is a closed circuit pressurized tunnel, with a confined square test section, 1.5 m in width and 4.5 m in length, enclosed in a plenum.

The adopted geometric conventions are shown in Fig. 1; taking also into account the tests carried out in Ref. 8, the relative position between wing and canards was chosen to be characterized by a fixed stagger of 2.26 wing mean geometric chords, and vertical positions with gaps T/L (Fig. 1) of -0.166, 0, and 0.166 (low, medium, and high positions). In the present Note no cases with decalage angles are considered.

One of the wing models already tested in Ref. 1 was used; it is a wing with zero twist and dihedral angles, aspect ratio 5.7, taper ratio 0.4, sweep angle $\Lambda = -25$ deg at $\frac{1}{4}$ of the chord, and a NACA 0012 wing section. The canard model was a unswept rectangular lifting surface with zero twist and dihedral angles, aspect ratio 4, NACA 0012 wing section, and a span of 0.47 times the wing span.

Due to the basic nature of the research, special attention was paid to the effects produced on the wing by the canard, and therefore the measurements were performed only on the wing at Mach numbers of 0.3 and 0.7, with a Reynolds number $\approx 2.8 \times 10^6$. Test conditions, model characteristics, and pressure orifice (0.5-mm diam) location are described in Ref. 1.

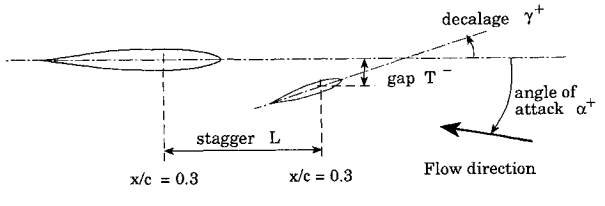

Fig. 1 Geometric conventions.